Annals of Glaciology 59(76pt1) 2018 doi: 10.1017/aog.2017.45

Ocean access beneath the southwest tributary of Pine Island Glacier, West Antarctica

Dustin M. SCHROEDER,[1,2] Andrew M. HILGER,[2] John D. PADEN,[3] Duncan A. YOUNG,[4] Hugh F. J. CORR[5]

[1]*Department of Geophysics, Stanford University, Stanford, CA, USA*
E-mail: dustin.m.schroeder@stanford.edu
[2]*Department of Electrical Engineering, Stanford University, Stanford, CA, USA*
[3]*Center for the Remote Sensing of Ice Sheets, University of Kansas, Lawrence, KS, USA*
[4]*Institute for Geophysics, University of Texas, Austin, TX, USA*
[5]*British Antarctic Survey, Natural Environment Research Council, Cambridge, UK*

ABSTRACT. The catchments of Pine Island Glacier and Thwaites Glacier in the Amundsen Sea Embayment are two of the largest, most rapidly changing, and potentially unstable sectors of the West Antarctic Ice Sheet. They are also neighboring outlets, separated by the topographically unconfined eastern shear margin of Thwaites Glacier and the southwest tributary of Pine Island Glacier. This tributary begins just downstream of the eastern shear margin and flows into the Pine Island ice shelf. As a result, it is a potential locus of interaction between the two glaciers and could result in cross-catchment feedback during the retreat of either. Here, we analyze relative basal reflectivity profiles from three radar sounding survey lines collected using the UTIG HiCARS radar system in 2004 and CReSIS MCoRDS radar system in 2012 and 2014 to investigate the extent and character of ocean access beneath the southwest tributary. These profiles provide evidence of ocean access ~12 km inland of the 1992–2011 InSAR-derived grounding line by 2014, suggesting either retreat since 2011 or the intrusion of ocean water kilometers inland of the grounding line.

KEYWORDS: glaciological instruments and methods, ground-penetrating radar, ice/ocean interactions, radio-echo sounding, remote sensing

INTRODUCTION

The Amundsen Sea Embayment (ASE) in West Antarctica has been described as the weak underbelly of the West Antarctic Ice Sheet because the landward-sloping beds of its two largest glaciers (Thwaites and Pine Island, Fig. 1) reach deep into the interior of the ice sheet, making them potentially vulnerable to unstable retreat (Hughes, 1981; Schoof, 2007; Alley and others, 2015; Scambos and others, 2017). The ASE is also the site of recent acceleration, surface lowering, and mass loss (Shepherd, 2001; Bamber and Rignot, 2002; Rignot and others, 2002; Joughin and others, 2003; Chen and others, 2009; Wingham and others, 2009; MacGregor and others, 2012; Mouginot and others, 2014) correlated with ice-shelf melting and the local intrusion of warm ocean water onto the continental shelf (Pritchard and others, 2009; Joughin and others, 2010; Rignot and others, 2013; Alley and others, 2015). These observations have raised the possibility that the unstable retreat of Thwaites Glacier and/or Pine Island Glacier may be underway (Joughin and others, 2014; Rignot and others, 2014). However, despite their dynamic character, potential instability, and immediate adjacency, most recent observational and modeling work has focused on either Pine Island (e.g., Joughin and others 2009; Scott and others 2009; Morlighem and others 2010; Gladstone and others 2012; Schodlok and others 2012; Dutrieux and others 2013, 2014a; Muto and others 2016; Brisbourne and others 2017) or Thwaites (e.g., Joughin and others 2009; Tinto and Bell 2011; MacGregor and others 2013; Parizek and others 2013; Schroeder and others 2013, 2014a,b, 2016a,b; Scambos and others 2017; Seroussi and others 2017; Smith and others 2017) separately rather than emphasizing their potential as a coupled, interacting system.

One area where this independent treatment is likely inadequate is the southwest tributary of Pine Island Glacier (Fig. 1b) which flows from the Thwaites trunk into the Pine Island ice shelf (MacGregor and others, 2012). This tributary initiates just downstream of the eastern shear margin of Thwaites Glacier, which is both the boundary with the Pine Island catchment and is the only Thwaites shear margin whose position is not strongly controlled by basal topography (MacGregor and others, 2013). It then flows between two regions with low ice surface speeds (Rignot and others (2011), Fig. 1b) and frozen bed conditions (Joughin and others, 2009; Schroeder and others, 2016a) before reaching its InSAR-derived grounding line (Rignot and others, 2014) just inland of the Pine Island ice-shelf edge (MacGregor and others, 2012). According to InSAR observations, the grounding-line location of the southwest tributary was stable between 1992 and 2011 (Rignot and others, 2014). However, recent observations and modeling of ocean-driven melting of the Pine Island Ice Shelf (Jenkins and others, 2010; Joughin and others, 2010; Pritchard and others, 2012; Schodlok and others, 2012; Dutrieux and others, 2013, 2014a,b; Park and others, 2013; Favier and others, 2014) make active melting beneath the southwest tributary of Pine Island Glacier appear likely or imminent. It is the aim of this paper is to exploit existing airborne radar sounding profiles (Fig. 1b) to evaluate the current extent of ocean access beneath the tributary.

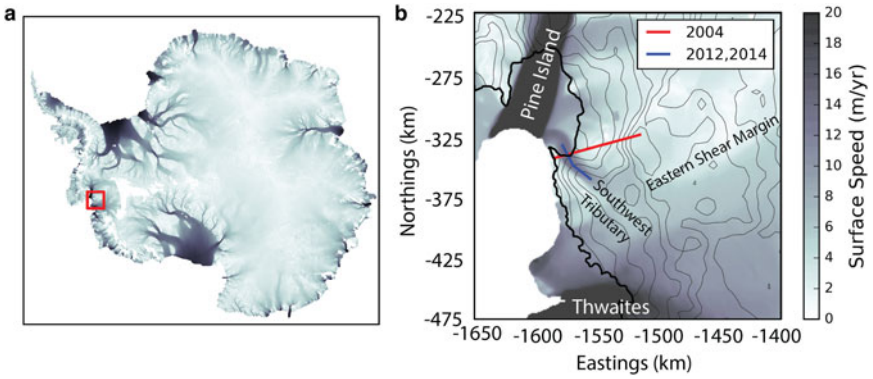

Fig. 1. (a) Our study area (red square and Figure 1b) in the context of ice surface speed from Rignot and others 2011 and ice-thickness contours from Fretwell and others 2013 in polar stereographic projection. (b) Flight lines for 2004 HiCARS (red) as well as 2012 and 2014 MCoRDS (blue) observations of the southwest tributary. 2011 grounding line (black) adapted from Rignot and others (2014).

METHOD AND RESULTS

In order to assess the reach and effect of ocean water beneath the southwest tributary, we investigate the relative reflectivity of two along-flow radar sounding profiles collected as part of NASA's Operation IceBridge (Koenig and others, 2011) using the CReSIS MCoRDS radar system (Li and others, 2013) in 2012 (Fig. 2a) and 2014 (Fig. 2d) (Table 1). The data used for this study were standard 195 MHz L1B CSARP processed radargrams (as used in MacGregor and others 2015a; Chu and others 2016; Jordan and others 2016; Khazendar and others 2016) with a wider bandwidth and larger cross-track antenna array used in 2014 (evident in Fig. 2). As part of this investigation, we identify potential along-flow step-changes in reflectivity (i.e. >~10 dB) consistent with a transition from ice-on-thawed-bed to ice-on-ocean reflectivity (Peters and others, 2005) in the same manner as Khazendar and others (2016).

To produce relative reflectivity profiles for the 2012 (Fig. 2c) and 2014 (Fig. 2f) MCoRDS profiles, we extract the bed-echo power from the MCoRDS radargrams (Figs 2a, d, respectively), correct for geometric spreading losses, and perform correlation-based attenuation-rate fitting for each profile (Fig. 3). We use the entire profile as a fitting window but otherwise follow Schroeder and others (2016b) to ensure the initial and post-correction correlations between bed-echo power and thickness satisfy the requirements (minimum and maximum respectively) for fitting and correcting attenuation for a short, outlet-glacier profile using this technique (Schroeder and others, 2016b). We reference the along-track distance of the MCoRDS profiles to a common, arbitrary point on the floating ice and take the bed-echo strength to be the strongest echo within a + or − 20 pixel window of the CReSIS bed picks (Fig. 2b for 2012 and 2e for 2014). We estimate the maximum and minimum attenuation rates for each profile as the maximum and minimum attenuation rates with correlation values <0.1 (Fig. 3). The resulting maximum and minimum relative reflectivity profiles are shown as the bounds on the gray-shaded area in Figures 2c, f.

In addition to the two repeat MCoRDS along-flow profiles discussed above (Fig. 2), we also analyzed a 2004 UTIG HiCARS radar profile (Fig. 4) which intersects the MCoRDS lines (Fig. 1b) in the vicinity of the grounding zone. The radar data used in this portion of the analysis were a standard 60 MHz UTIG HiCARS unfocused SAR radar sounding profiles (as used in Schroeder and others (2014a, 2016a,b)) (Table 1). We follow the same attenuation-rate fitting procedure (Fig. 3) as described above for the MCoRDS data to produce maximum and minimum relative reflectivity profiles (bounding the gray region shown in Fig. 4b). The wider (larger uncertainty) attenuation-fitting curve in Figure 3 with a similar minimum-correlation estimated attenuation rate is fully consistent with two sounding profiles through the same area of the ice sheet with steady and significant along-track topographic relief (Figs 2, 3) for one profile and more modest and constrained relief for the other (Figs 3, 4). For this paper, we deliberately chose not to cross-calibrate or absolutely register the relative reflectivity profiles profiles calculated for the HiCARS (Fig. 4) and MCoRDS (Fig. 2) data. Therefore, the profiles for each system (which will have different means since they span different bed reflectivity regions) must be interpreted independently (as relative profiles) before those interpretations (rather than specific relative reflectivity values) are compared at their crossing points (Fig. 1 and dashed lines in Figs 4, 5).

By contrast, because we are interested primarily in interpreting changes in along-profile reflectivity in a two repeat-track MCoRDS radargrams (Fig. 1b) with the same extent (Fig. 2), we are able quantitatively compare their relative reflectivity by assuming that the mean reflectivity over the profile is unchanged. This assumption is supported by the close match of relative reflectivity values inland of the 18 km along the track distance point (Figs 2, 5). This is further supported by the similarity of the attenuation fitting curves for both lines (Fig. 3) and the range of resulting reflectivity values (Figs 2c, f) despite the differences in system parameters and/or processing apparent in their corresponding radargrams (Figs 2a, d). Figure 5b shows the change in reflectivity between 2012 and 2014 for both the minimum and maximum attenuation rates (range shown in gray).

DISCUSSION

There have been recent advances in combining observations from multiple radar-sounding surveys to constrain ice-sheet temperature (MacGregor and others, 2015b), age (MacGregor and others, 2015a), map subglacial and englacial conditions (Jordan and others, 2016, 2017), and detect temporal changes in subglacial hydrology (Chu and others, 2016) or ice-shelf melt (Khazendar and others, 2016). However, to our knowledge, no study has done so with data from two or more different families of radar systems. This will be required

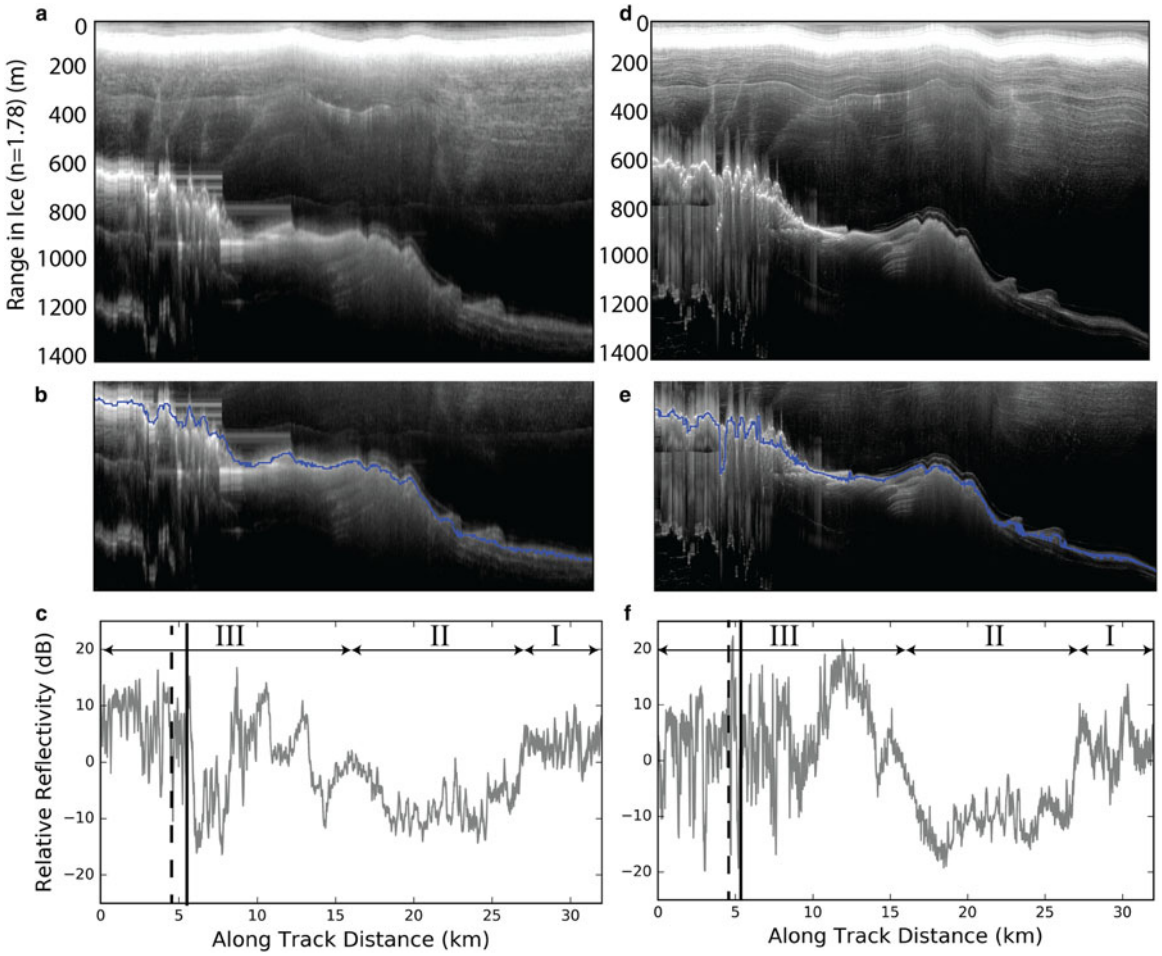

Fig. 2. MCoRDS radargrams from (a) 2012 and (d) 2014, their corresponding bed picks (b, e), and relative reflectivity profiles (c, f). Gray-shaded plots show the range between the maximum and minimum relative reflectivity profiles from attenuation-rate fitting (Fig. 3). Zones I, II, and III correspond to areas of moderate, lower, and higher relative reflectivity values moving from the landward to seaward direction. The dashed black line shows the intersection with the 2004 HiCARS flight line (Fig. 4). The black white line shows the location of the 1992–2011 InSAR-derived grounding line (Rignot and others, 2014).

if continent-scale studies are carried out in Antarctica due to the comparative heterogeneity of extant data relative to Greenland (Pritchard, 2014). This paper is a first attempt to do so by utilizing data from two different radar systems (HiCARS and MCoRDS) in a quantitative analysis of bed-echo power in order to answer the specific question of how far ocean water reaches beneath the southwest tributary of Pine Island Glacier.

This question is well suited to a first cross-system relative-reflectivity comparison since we have existing hypotheses for the expected reflectivity transitions for across-flow and along-flow lines. For the along-flow lines, we expect to see transitions of >10–20 dB associated with the transition from a grounded, thawed bed to floating ice (Peters and others, 2005; Khazendar and others, 2016; Schroeder and others, 2016a), which is consistent with the observed ~20 dB range in relative reflectivity values in Figure 2. For the across-flow line, we expect to see transitions of 30 dB from a grounded, frozen bed to floating ice (due to the greater reflectivity contrast for this transition; Peters and others 2005; Schroeder and others 2016a), which is consistent with the observed ~30 dB range in relative reflectivity values in Figure 4.

Table 1. Radar-sounding data used in this paper

Radar system	Year	Profile name	Processing
MCoRDS	2012	Data 20121104 05 036	CSARP standard
MCoRDS	2014	Data 20141029 05 036	CSARP standard
HiCARS	2004	THW/SJB2/X79a	Unfocused SAR

By inspecting individual relative reflectivity profiles, it is clear that the 2004 cross-flow profile (Fig. 4b) crosses an ~10 km wide stretch of floating ice between two areas of frozen bed (consistent with Joughin and others 2009 and Schroeder and others 2016a). The floating portion of this profile also, unsurprisingly, crosses the along-flow profiles (Fig. 1 and dashed lines in Figs 4, 5) seaward of the 1992-2011 InSAR-derived grounding line (Rignot and others (2014) and solid white line in Fig. 5). It is also clear that the 2012 and 2014 profiles (Figs 2c, e) cross three distinct regions (moving from the landward to seaward side of the figure): (I) a moderate relative reflectivity region (~0 dB) from 32 to ~20 km along track; (II) a low relative reflectivity region (~−10 dB) from ~20 to ~15 km along track; and (III) a region of increasing relatively reflectivity starting from that low value (~ − 10 dB) and reaching the highest values (~10 dB) from ~15 to 0 km along track. We interpret these regions (from seaward to landward) as (III) floating ice, (II) grounded thawed bed, and (I) grounded thawed bed with greater quantities of subglacial water (than region II)

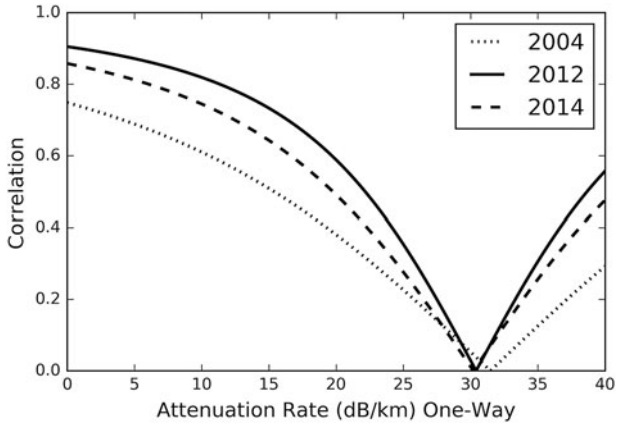

Fig. 3. Fitting curves for englacial attenuation (after Schroeder and others (2016b)) for the 2004 HiCARS profile shown in Figure 4 as well as the 2012 and 2014 MCoRDS profiles shown in Figure 2.

landward of the basal topographic high at ~18 km (consistent with Peters and others 2005; Joughin and others 2009; Schroeder and others 2013, 2016a; Khazendar and others 2016; Smith and others 2017).

Beyond the individual reflectivity profiles, the change in relative reflectivity between the 2012 and 2014 repeat MCoRDS profiles (Fig. 5b) shows that while neither of the inland regions (I and II above) experienced a significant change in reflectivity, the reflectivity of entire region seaward of ~18 km along track either increased (blue areas in Fig. 5) or decreased (red areas in Fig. 5) by ~10 dB. Additionally, the point where the 2004 across-flow line crosses the along-flow lines (dashed lines in Figs 4, 5) had high relative reflectivity values in 2004 and 2014 (Fig. 2e), but was lower (than 2014) in 2012 (Figs 2c, 5). We interpret these

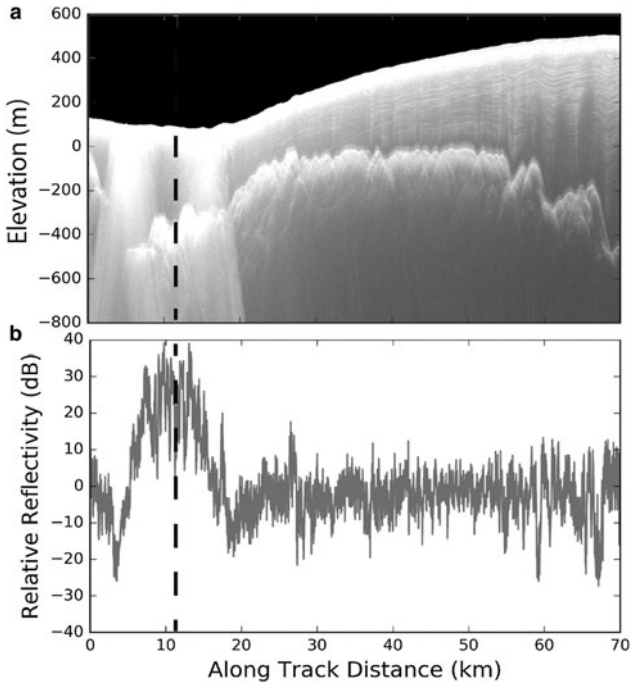

Fig. 4. (a) 2004 HiCARS radargram and (b) relative reflectivity profile. Gray-shaded plot show the range between the maximum and minimum relative reflectivity profiles from attenuation-rate fitting (Fig. 3). Dashed line shows location of the intersection with MCoRDS flight lines (Fig. 2).

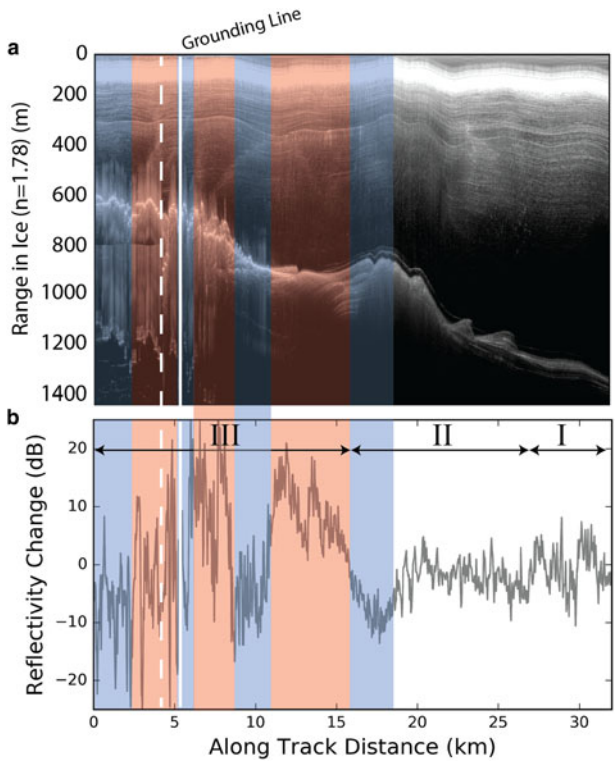

Fig. 5. (a) The 2014 MCoRDS radargram and (b) change in relative reflectivity between 2012 and 2014. Areas of reflectivity decrease are shown in blue and areas of reflectivity increase are shown in red. Gray-shaded plot shows the range between the maximum and minimum reflectivity change. The dashed white line shows the intersection with the 2004 HiCARS flight line (Fig. 4). The solid white line shows the location of the 1992–2011 InSAR-derived grounding line (Rignot and others, 2014) Zones I, II, and III correspond to areas of moderate, lower, and higher relative reflectivity values moving from the landward to the seaward direction.

intermittent increases and decreases to be the competing effects of basal melting (which can strengthen reflections from floating ice by smoothing the basal interface) and basal crevassing or accretion (which can weaken reflections from floating ice by increasing roughness) (Peters and others, 2005; MacGregor and others, 2013; Greenbaum and others, 2015; Schroeder and others, 2015) or discontinuous grounding and/or ocean water exclusion (e.g. Horgan and others 2013; Parizek and others 2013; Walker and others 2013; Sugiyama and others 2014; Khazendar and others 2016), but consider all of these to be expressions of ocean access. Therefore, we place the extent of ocean access by 2014 to be around the 18 km point and ~13 km inland of the 2011 InSAR-derived grounding line (Rignot and others 2014 and solid line in Fig. 5). This suggests that either the grounding line has retreated beyond its apparently stable 1992–2011 position (Rignot and others, 2014) or that ocean water and related processes have access significantly (kilometers) inland of the InSAR-derived grounding line (e.g. Horgan and others 2013; Parizek and others 2013; Walker and others 2013; Greenbaum and others 2015; Khazendar and others 2016).

CONCLUSIONS

By comparing relative basal reflectivity profiles from three radar-sounding survey lines collected using the UTIG HiCARS

radar system in 2004 and the CReSIS MCoRDS radar system in 2012 and 2014, we find evidence of a dynamic grounding zone with ocean access (including areas of both increased reflectivity from ocean intrusion or basal melting and decreased reflectivity from crevassing, accretion, or ocean water exclusion) ~13 km inland of the 1992–2011 InSAR-derived grounding line. This suggests that, as ocean-driven melting and retreat of Pine Island Glacier progresses, warm ocean water will have increasing access beneath the southwest tributary and may propagate inland of the currently frozen portion of the Thwaites Glacier grounding line, potentially triggering or facilitating retreat in that catchment as well.

ACKNOWLEDGMENTS

D.M.S. was partially supported by a grant from the NASA Cryospheric Sciences Program. This is UTIG contribution 3200.

REFERENCES

Alley RB and 7 others (2015) Oceanic forcing of ice-sheet retreat: West Antarctica and more. *Annu. Rev. Earth Planet. Sci.*, **43**(1), 207–231

Bamber J and Rignot E (2002) Unsteady flow inferred for Thwaites Glacier, and comparison with Pine Island Glacier, West Antarctica. *J. Glaciol.*, **48**(161), 237–246

Brisbourne AM and 8 others (2017) Bed conditions of Pine Island Glacier, West Antarctica. *J. Geophys. Res.: Earth Surf.*, **122**(1), 419–433

Chen JL, Wilson CR, Blankenship D and Tapley BD (2009) Accelerated Antarctic ice loss from satellite gravity measurements. *Nat. Geosci.*, **2**(12), 859–862

Chu W and 5 others (2016) Extensive winter subglacial water storage beneath the Greenland Ice Sheet. *Geophys. Res. Lett.*, **43**(24), 484–492

Dutrieux P and 6 others (2013) Pine Island Glacier ice shelf melt distributed at kilometre scales. *Cryosphere*, **7**(5), 1543–1555

Dutrieux P and 9 others (2014a) Strong sensitivity of Pine Island ice-shelf melting to climatic variability. *Science*, **343**(6167), 174–178

Dutrieux P and 6 others (2014b) Basal terraces on melting ice shelves. *Geophys. Res. Lett.*, **41**(15), 5506–5513

Favier L and 8 others (2014) Retreat of Pine Island Glacier controlled by marine ice-sheet instability. *Nat. Clim. Chang.*, **4**(2), 117–121

Fretwell P and 59 others (2013) Bedmap2: improved ice bed, surface and thickness datasets for Antarctica. *The Cryosphere*, **7** (1), 375–393

Gladstone RM and 9 others (2012) Calibrated prediction of Pine Island Glacier retreat during the 21st and 22nd centuries with a coupled flowline model. *Earth. Planet. Sci. Lett.*, **333–334**, 191–199

Greenbaum JS and 10 others (2015) Ocean access to a cavity beneath Totten Glacier in East Antarctica. *Nat. Geosci.*, **8**(4), 294–298

Horgan HJ and 7 others (2013) Estuaries beneath ice sheets. *Geology*, **41**(11), 1159–1162

Hughes TJ (1981) The weak underbelly of the West Antarctic ice-Sheet. *J. Glaciol.*, **27**(97), 518–525

Jenkins A and 6 others (2010) Observations beneath Pine Island Glacier in West—[nbsp]—Antarctica and implications for its retreat. *Nat. Geosci.*, **3**(7), 468–472

Jordan TM and 7 others (2016) An ice-sheet-wide framework for englacial attenuation from ice-penetrating radar data. *Cryosphere*, **10**(4), 1547–1570

Jordan TM and 6 others (2017) Self-affine subglacial roughness: consequences for radar scattering and basal water discrimination in northern Greenland. *Cryosphere*, **11**(3), 1247–1264

Joughin I, Rignot E, Rosanova CE, Lucchitta BK and Bohlander J (2003) Timing of recent accelerations of Pine Island Glacier, Antarctica. *Geophys. Res. Lett.*, **30**(13), 1706

Joughin I and 6 others (2009) Basal conditions for Pine Island and Thwaites Glaciers, West Antarctica, determined using satellite and airborne data. *J. Glaciol.*, **55**(190), 245–257

Joughin I, Smith BE and Holland DM (2010) Sensitivity of 21st century sea level to ocean-induced thinning of Pine Island Glacier, Antarctica. *Geophys. Res. Lett.*, **37**(20), L20502

Joughin I, Smith BE and Medley B (2014) Marine ice sheet collapse potentially under way for the Thwaites Glacier Basin, West Antarctica. *Science*, **344**(6185), 735–738

Khazendar A and 8 others (2016) Rapid submarine ice melting in the grounding zones of ice shelves in West Antarctica. *Nat. Commun.*, **7**

Koenig L, Martin S, Studinger M and Sonntag J (2011) Polar Airborne Observations Fill Gap in Satellite Data. *Eos, Trans. Amer. Geophys. Union*, **91**(38), 333–334

Li J and 8 others (2013) High-altitude radar measurements of ice thickness over the Antarctic and Greenland ice sheets as a part of operation IceBridge. *IEEE Trans. Geosci. Remote. Sens.*, **51** (2), 742–754

MacGregor JA, Catania GA, Markowski MS and Andrews AG (2012) Widespread rifting and retreat of ice-shelf margins in the eastern Amundsen Sea Embayment between 1972 and 2011. *J. Glaciol.*, **58**(209), 458–466

MacGregor JA and 7 others (2013) Weak bed control of the eastern shear margin of Thwaites Glacier, West Antarctica. *J. Glaciol.*, **59** (217), 900–912

MacGregor JA and 9 others (2015a) Radiostratigraphy and age structure of the Greenland Ice Sheet. *J. Geophys. Res.: Earth Surface*, **120**(2), 212–241

MacGregor JA and 11 others (2015b) Radar attenuation and temperature within the Greenland Ice Sheet. *J. Geophys. Res.: Earth Surface*, **120**(6), 983–1008

Morlighem M and 5 others (2010) Spatial patterns of basal drag inferred using control methods from a full-Stokes and simpler models for Pine Island Glacier, West Antarctica. *Geophys. Res. Lett.*, **37**(14), L14502

Mouginot J, Rignot E and Scheuchl B (2014) Sustained increase in ice discharge from the Amundsen Sea Embayment, West Antarctica, from 1973 to 2013. *Geophys. Res. Lett.*, **41**(5), 1576–1584

Muto A and 6 others (2016) Subglacial bathymetry and sediment distribution beneath Pine Island Glacier ice shelf modeled using aerogravity and in situ geophysical data: New results. *Earth. Planet. Sci. Lett.*, **433**, 63–75

Parizek BR and 10 others (2013) Dynamic (in)stability of Thwaites Glacier, West Antarctica. *J. Geophys. Res.: Earth Surf.*, **118**(2), 638–655

Park JW and 5 others (2013) Sustained retreat of the Pine Island Glacier. *Geophys. Res. Lett.*, **40**(10), 2137–2142

Peters ME, Blankenship DD and Morse DL (2005) Analysis techniques for coherent airborne radar sounding: Application to West Antarctic ice streams. *J. Geophys. Res.: Solid Earth*, **110**(B6), B06303

Pritchard HD (2014) Bedgap: where next for Antarctic subglacial mapping? *Antarct. Sci.*, **26**(06), 742–757

Pritchard HD, Arthern RJ, Vaughan DG and Edwards LA (2009) Extensive dynamic thinning on the margins of the Greenland and Antarctic ice sheets. *Nature*, **461**(7266), 971–975

Pritchard HD and 5 others (2012) Antarctic ice-sheet loss driven by basal melting of ice shelves. *Nature*, **484**(7395), 502–505

Rignot E, Vaughan DG, Schmeltz M, Dupont TK and MacAyeal D (2002) Acceleration of Pine island and Thwaites glaciers, west Antarctica. *Ann. Glaciol.*, **34**(1), 189–194

Rignot E, Mouginot J and Scheuchl B (2011) Ice flow of the Antarctic ice sheet. *Science*, **333**(6048), 1427–1430

Rignot E, Jacobs S, Mouginot J and Scheuchl B (2013) Ice-shelf melting around Antarctica. *Science*, **341**(6143), 266–270

Rignot E, Mouginot J, Morlighem M, Seroussi H and Scheuchl B (2014) Widespread, rapid grounding line retreat of Pine Island, Thwaites, Smith, and Kohler glaciers, West Antarctica, from 1992 to 2011. *Geophys. Res. Lett.*, **41**(10), 3502–3509

Scambos TA and 22 others (2017) How much, how fast?: A science review and outlook for research on the instability of Antarctica's Thwaites Glacier in the 21st century. *Glob. Planet. Change*, **153**, 16–34

Schodlok MP, Menemenlis D, Rignot E and Studinger M (2012) Sensitivity of the ice-shelf/ocean system to the sub-ice-shelf cavity shape measured by NASA IceBridge in Pine Island Glacier, West Antarctica. *Ann. Glaciol.*, **53**(60), 156–162

Schoof C (2007) Ice sheet grounding line dynamics: Steady states, stability, and hysteresis. *J. Geophys. Res.: Solid Earth*, **112**(F3), F03S28

Schroeder DM, Blankenship DD and Young DA (2013) Evidence for a water system transition beneath Thwaites Glacier, West Antarctica. *Proc. Natl. Acad. Sci. USA*, **110**(30), 12225–12228

Schroeder DM, Blankenship DD, Young DA and Quartini E (2014a) Evidence for elevated and spatially variable geothermal flux beneath the West Antarctic Ice Sheet. *Proc. Natl. Acad. Sci. USA*, **111**(25), 9070–9072

Schroeder DM, Blankenship DD, Young DA, Witus AE and Anderson JB (2014b) Airborne radar sounding evidence for deformable sediments and outcropping bedrock beneath Thwaites Glacier, West Antarctica. *Geophys. Res. Lett.*, **41**(20), 7200–7208

Schroeder DM, Blankenship DD, Raney RK and Grima C (2015) Estimating subglacial water geometry using radar bed echo specularity: application to Thwaites Glacier, West Antarctica. *IEEE Geosci. Remote. Sens. Lett.*, **12**(3), 443–447

Schroeder DM, Grima C and Blankenship DD (2016a) Evidence for variable grounding-zone and shear-margin basal conditions across Thwaites Glacier, West Antarctica. *Geophysics*, **81**(1), WA35–WA43

Schroeder DM, Seroussi H, Chu W and Young DA (2016b) Adaptively constraining radar attenuation and temperature across the Thwaites Glacier catchment using bed echoes. *J. Glaciol.*, **62** (236), 1075–1082

Scott JBT and 5 others (2009) Increased rate of acceleration on Pine Island Glacier strongly coupled to changes in gravitational driving stress. *Cryosphere*, **3**(1), 125–131

Seroussi H, Ivins ER, Wiens DA and Bondzio J (2017) Influence of a West Antarctic mantle plume on ice sheet basal conditions. *J. Geophys. Res.: Solid Earth*, **122**(9), 7127–55

Shepherd A (2001) Inland thinning of Pine Island Glacier, West Antarctica. *Science*, **291**(5505), 862–864

Smith BE, Gourmelen N, Huth A and Joughin I (2017) Connected subglacial lake drainage beneath Thwaites Glacier, West Antarctica. *Cryosphere*, **11**(1), 451–467

Sugiyama S, Sawagaki T, Fukuda T and Aoki S (2014) Active water exchange and life near the grounding line of an antarctic outlet glacier. *Earth. Planet. Sci. Lett.*, **399**(Suppl. C), 52–60

Tinto KJ and Bell RE (2011) Progressive unpinning of Thwaites Glacier from newly identified offshore ridge: Constraints from aerogravity. *Geophys. Res. Lett.*, **38**(20), L20503

Walker RT and 5 others (2013) Ice-shelf tidal flexure and subglacial pressure variations. *Earth. Planet. Sci. Lett.*, **361**, 422–428

Wingham DJ, Wallis DW and Shepherd A (2009) Spatial and temporal evolution of Pine Island Glacier thinning, 1995–2006. *Geophys. Res. Lett.*, **36**(17), L17501